ISSN 1392 - 1207. MECHANIKA. 2013 Volume 19(6): 649-656

The effects of operating parameters on the performance of proton exchange membrane fuel cells

M. Dehsara*, M.J. Kermani**

**Department of Mechanical Engineering, Amirkabir University of Technology (Tehran Polytechnic), 424 Hafez Avenue, P.O. Box, 15875-4413 Tehran, Iran, E-mail: bm_dehsara@aut.ac.ir*

***Energy Conversion Research Laboratory, and The New Technologies Research Center, Department of Mechanical Engineering, Amirkabir University of Technology (Tehran Polytechnic), 424 Hafez Avenue, P.O. Box, 15875-4413 Tehran, Iran, E-mail: mkermai@aut.ac.ir*

crossref http://dx.doi.org/10.5755/j01.mech.19.6.5989

Nomenclature

A_g - generation area, m^2; $C_{O_2}^{ref}$ - reference Oxygen concentration, mol/m^3; D_{O_2} - reference diffusivity of O_2, m^2/s; D_{H_2O} - reference diffusivity of H_2O, m^2/s; F - Faraday number; h_{ch} - channel height, m; h_{GDL} - gas diffusion layer (GDL) height, m; h_{CL} - catalyst layer (CL) height, m; i - current density, A/m^2; j - diffusion mass flux, kg/m^2.s; K - hydraulic permeability of GDL and CL, m^2; L_{ch} - channel length, m; M - molecular mass, kg/mol; P - pressure vector, Pa; R - universal gas constant, J/(kg mol K); S - source term; T - temperature, K; $\vec{V}$ - velocity, m/s; V_{cell} - fuel cell working voltage, V; V_g - computational cell volume, m^3; V_{oc} - open-circuit voltage, V; y - mass fraction.

Greek symbols:

α_c - cathode exchange coefficient; ε_{CL} - porosity of CL; ε_{GDL} - porosity of GDL; η_{act} - activation voltage, V; ρ - mixture density, kg/m^3; σ - Ohmic resistance, m^2.

Subscripts:

act - activation; *CL* - catalyst layer; *GDL* - gas diffusion layer; *i* - component of the mixture.

1. Introduction

The wide range of applications from cell phones to new vehicle generation makes proton exchange membrane fuel cells (PEMFCs) a distinguished type fuel cells, expected to play a key role in the future energy system. PEMFCs combine the advantages of running on low operating temperature, high energy efficiency and low pollution levels. Improving the performance and reducing the cost of the fuel cells are generally main development aspects that researchers are working on. Due to PEMFC especial dimensions, access to inner parts of the cell to measure flow quantities, is hardly possible. Alternative, another possibility for detailed study of species concentrations or temperature field through the components of PEMFC is the use of computational fluid dynamics (CFD) software packages.

Many researchers have focused on different aspects of PEMFCs by experimental works. Wang and Liu [1] presented systematic experimental data on the performance of a proton exchange membrane fuel cell. Their experiments concentrated on the effects of cell temperature, gas humidification, cell operating pressure and reactant gas flow rate. And the results are shown in the form of polarization curves. Jordan et al. [2] presented the gas diffusion layer parameters effects on polymer electrolyte fuel cell performances. Sridhar and his colleagues [3] studied PEMFCs performance by two methods of humidifying. At the same time many models have been simulated to study PEMFC performance. Gurau et al. [4] presented mathematical model which enables prediction of phenomena in entire PEM fuel cell. Sun et al. [5] investigated a single-phase, cathode side model to account for structural parameters. COMSOL Multiphysics (FEMLAB) was used to solve all governing equations in general form. A non-isothermal, single-phase model was presented by Litster et al. [6]. They addressed heat and mass transfer on the cathode side of the fuel cell. The model was solved using CFX and the SIMPLEC algorithm.

Many parameters influence the performance of proton exchange membrane (PEM) fuel cells such as operating pressure and temperature so that it is important studies these effects to improve fuel cells' performance. In this paper, a two-dimensional numerical computation of steady, compressible, isothermal and single-phase flow of reactant–product gases mixture in the air side electrode of PEMFC is performed. The mixture is composed of three species including oxygen, water vapor and nitrogen. The model presented in this paper is a typical three-zone that consists of cathode-side gas flow channel, cathode-side gas diffusion layer and cathode-side catalyst layer. The effects of operating and geometric parameters on the performance of PEMFCs are studied. The numerical model of the present paper is validated using the available experimental data.

2. Numerical modelling

For the present computation the assembly of the software packages Gambit+Fluent has been used. The geometry employed here is generated using the software Gambit. Then the problem is run and solved in the software Fluent using the UDFs developed by the author in the C programming language.

Fig. 1 shows the schematic of a computational unit of PEM fuel cell with straight-channel-bed. Layers of the computational unit include cathode flow channel, gas diffusion layer (GDL), and catalyst layer (CL).

Structured types of grids (in the form of quad elements) are applied to each three zones of the computa-

tional unit. To solve the problem, main assumptions considered here are:

- the PEMFC performs under steady-state conditions;
- the reacting gas mixtures are regarded as ideal gases;
- the gas flow is laminar and compressible;
- the GDL and CL are treated as isotropic porous media.

The governing equations used in the present study are given next.

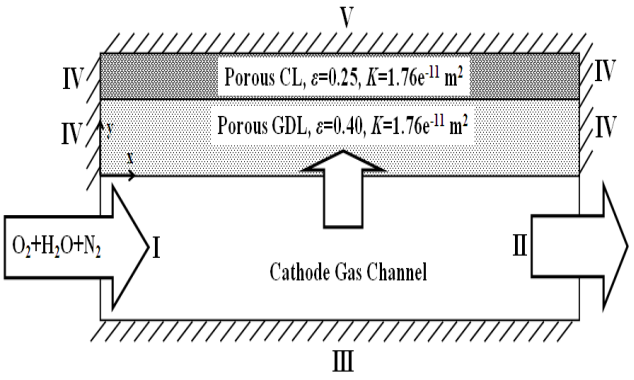

Fig. 1 Schematics of the computational unit

3. Governing equations

The governing equations of the PEMFCs are described below.

3.1. Conservation equations of mass and momentum

The mixture continuity equation for the present steady computation is governing by:

$$\nabla\left(\varepsilon\rho\vec{V}\right)=0, \tag{1}$$

where ε is the porosity of the GDL and CL (Table 1 for the values), $\vec{V}$ is the mixture mass averaged velocity and ρ is the mixture density which can be defined as:

$$\rho=\frac{1}{\sum\left(y_i/\rho_i\right)}, \tag{2}$$

where y_i is the mass fraction of the i-th component of the mixture. The density of each component is determined using the ideal gas law:

$$\rho_i=\frac{PM_i}{RT}, \tag{3}$$

where P is pressure, M_i is molecular mass, T is temperature and R is the universal gas constant.

The flow field is uniquely determined by the Navier-Stokes equations which express the momentum conservation for a Newtonian fluid. So the mixture momentum equation is given by:

$$\nabla\left(\varepsilon\rho\vec{V}\vec{V}\right)=-\varepsilon\nabla P+\nabla\left(\varepsilon\mu\nabla\vec{V}\right)+S_m, \tag{4}$$

where S_m is the momentum source term taken as $S_m=0$ in the gas flow channels. For the porous regions the source term $S_m=-\varepsilon^2\mu\vec{V}/K$, hence the momentum equation reduces to Darcy equation: $\varepsilon\vec{V}=-K\nabla P/\mu$, where μ is the dynamic viscosity of the mixture.

3.2. Species transport equations

The steady state species transport equation is written as follows:

$$\nabla\left(\varepsilon\vec{V}\rho_i\right)=\nabla\left(D_i^{eff}\nabla\rho_i\right)+S_i, \tag{5}$$

where S_i is the volumetric source terms for the species, which represents the generation/consumption of species i. $S_i=0$ for all of the layers except the catalyst layers which possess generation/consumption of the species:

$$S_{O_2}=-\frac{M_{\omega,O_2}i}{4F}\frac{A_g}{V_g}; \tag{6}$$

$$S_{H_2O}=+\frac{M_{\omega,H_2O}i}{2F}\frac{A_g}{V_g}, \tag{7}$$

where M is the molecular mass of one of the species, F is the Faraday constant, and i is the current density. A_g is the area from which the species i is generated, and V_g is the computational cell volume that consists sink and source terms.

3.3. Properties

The Bruggemann equation is used for the diffusion of gas species at the desired temperature, and pressure [7, 8]:

$$D_i=\varepsilon^{1.5}D_i^0\left(\frac{P_0}{P}\right)^{\gamma_p}\left(\frac{T}{T_0}\right)^{\gamma_t}, \tag{8}$$

where D_i^0 is the mass diffusion of species i at reference temperature and pressure (T_0, p_0), γ_p and γ_t are the reference and constant values.

3.4. Current calculation

To calculate the fuel cell current, the Butler-Volmer equation is used [9]:

$$\eta_{act}=\frac{RT}{\alpha_c F}ln\left(\frac{i}{i_{0,c}}\frac{C_{O_2}^{ref}}{C_{O_2}}\right), \tag{9}$$

where η_{act} is activation voltage, α_c is load transport coefficient of the cathode side, F is the Faraday constant, R is the universal gas constant, T is fuel cell operating temperature, C_{O_2} is oxygen molar concentration, and $i_{0,c}$ is the value of exchanged current in fuel cell no-load condition. In PEM fuel cell operating temperature range, the value of $i_{0,c}$ can be determined from [9]:

$$i_{0,c}=10^{6.507-4001/T}. \tag{10}$$

The molar concentration of oxygen is obtained using the following relation:

$$C_{O_2} = \frac{Y_{O_2}\rho}{M_{\omega,O_2}}. \quad (11)$$

In the present study, only the activation and ohmic losses are considered. Therefore the relation between V_{rev} and V_{cell} can be defined as:

$$V_{cell} = V_{rev} - i\sigma - \eta_{act}, \quad (12)$$

where σ is the fuel cell ohmic resistance, η_{act} is the activation voltage loss, V_{cell} is the fuel cell working voltage, and V_{rev} is the fuel cell open-circuit voltage. The relation between V_{cell} and the fuel cell working temperature is obtained using the following relation [9]:

$$V_{cell} = \frac{1}{229} - 0.85\times10^{-3}(T-298) + \\ + \frac{4}{31}\times10^{-5}T\left(ln\,P_{H_2} + \frac{1}{2}ln\,P_{O_2}\right). \quad (13)$$

By combining relations (9) and (12), can be written:

$$i = i_{0,c}\frac{C_{O_2}}{C_{O_2}^{ref}}exp\left(\frac{\alpha_c F}{RT}V_{rec} - V_{cell} - i\sigma\right). \quad (14)$$

Eq. (14) shows the relation among V_{rec}, V_{cell}, i and fuel cell internal conditions.

To obtain average current density from current density, the following relation is used:

$$I = \frac{1}{A_g}\int_{A_g} i.da, \quad (15)$$

where i is the current density, A_g is the area from which current density i is generated.

4. Boundary conditions

For the following discussion of boundary conditions, refer to Fig. 1.

- At the boundary location I (channel inlet) where the flow enters to the cathode channel, mass flow inlet condition is specified.
- At the boundary location II (channel exit) where the flow leaves the cathode channel, pressure outlet condition is specified.
- At boundary locations III to V, all of the surfaces are set to stationary walls.
- Cathode flow channel, GDL and CL are set to fluid zones.

5. Solution method

The representation of the mesh generation and geometry creation in the present computation are given in Fig. 2. As it can be seen, the grid network consists of three zones of cathode channel, GDL and CL that their interior surfaces are shown with the blue lines. A control volume method within the environment of software package Fluent has been used to solve the governing equations and perform the parametric studies in the present paper. The SIMPLE algorithm is taken for computation with 1×10^{-5} precision. The model consists of several user-defined functions (UDFs) to incorporate the formulations, source terms and other model parameters that are written by authors. Multigrid cycle is also set to F-Cycle for all the equations. Stabilization method is changed to BCGSTAB (bi-conjugate gradient stabilized method) for species concentrations. Also maximum number of cycles was increased for 50. The under-relaxation factors for the governing equations are set as follows: for pressure to 0.45, for density to 1, for body forces to 0.9, for momentum to 0.3, for species concentration to 0.9, for energy to 0.2. The discretization method was changed to second order (leading to more precise solutions) for all equations [10].

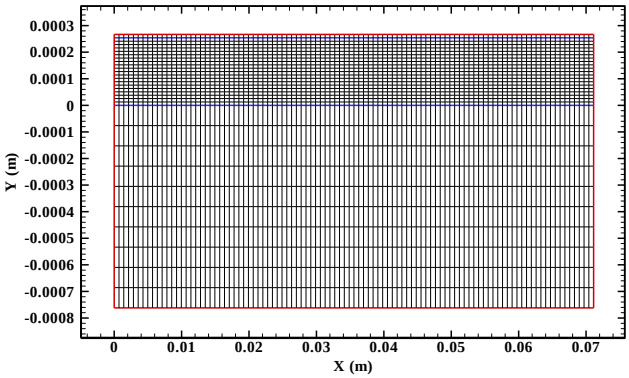

Fig. 2 Representation of the mesh generation and geometry creation in present computational unit

6. Results and discussion

In this paper, a two-dimensional numerical computation of steady, compressible, isothermal and single-phase flow of reactant–product gases in the air side electrode of PEMFC is performed. The effects of operating and geometric parameters on the performance of PEMFCs are studied. The PEM fuel cell operates at 80°C temperature, 5 atm pressure and relative humidity of 100%. Table 1 shows the physical parameters used in the present computation.

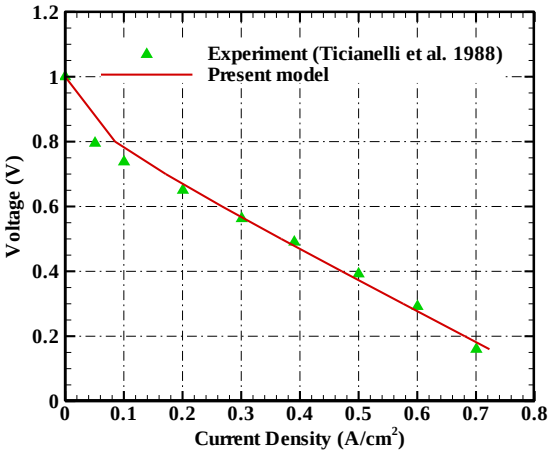

Fig. 3 Comparison of the numerical predictions and the experimental data [11] for polarization curves

Table 1

Physical properties and parameters

Symbol	Property	Value/Reference
L_{ch}	Channel length	7.112 cm
h_{ch}	Channel height	0.0762 cm
h_{GDL}	Gas diffusion layer height	0.0254 cm
h_{CL}	Catalyst layer height	0.00127 cm
ε_{GDL}	Porosity of GDL	0.4 [12]
K	Hydraulic permeability of GDL and CL	1.76×10^{-11} m^2 [13]
V_{oc}	Open circuit voltage	$0.0025T + 0.2329$ V [10]
α_c	Cathode exchange coefficient	1 [14]
D_{O_2}	Reference diffusivity of O_2	2.06×10^{-5} m^2/s
D_{H_2O}	Reference diffusivity of H_2O	2.56×10^{-5} m^2/s
ε_{CL}	Porosity of CL	0.25 [12]
σ	Ohmic resistance	0.55 Ω cm^2 [8]
$C_{O_2}^{ref}$	Reference oxygen concentration	1.2×10^{-6} mol cm^{-3} [14]

Fig. 3 depicts a comparison between the simulation results and the experimental data of Ticianelli et al. [11]. As it can be seen in Fig. 3, there is a good agreement between the polarization curves of numerical and experimental results, which confirms the validity of the present paper model.

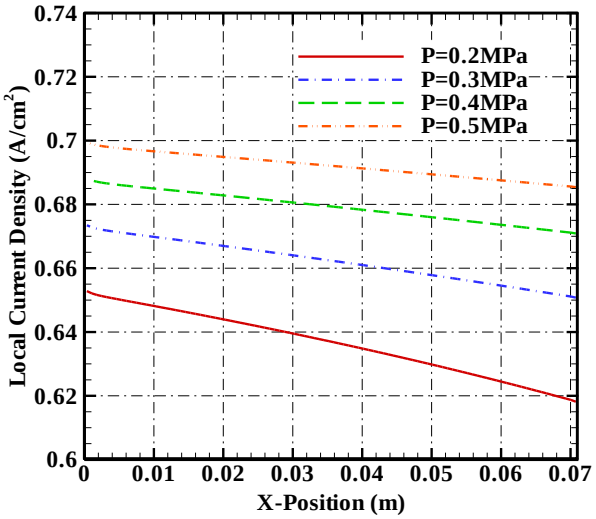

Fig. 4 The distribution of the local current density at middle of catalyst layer for different fuel cell pressure

Fig. 4 shows the variations of local current density with respect to operating pressure. As is can be observed, the local current generation increases with the increase of fuel cell pressure. The increase of pressure causes the increase of reacting gasses diffusion from GDL to the catalyst layer, and consequently the reaction rate in catalyst layer, which is the reaction site, increases. As a result, higher local current is generated.

The variations of oxygen sink term with respect to the fuel cell operating pressure are shown in Fig. 5. It can be seen that the oxygen consumption rate in catalyst layer increases with the increase of operating pressure. The increase of pressure causes the increase of oxygen diffusion in catalyst layer, which is the reaction site, and therefore the oxygen consumption rate increases due to the oxygen higher presence in reaction site.

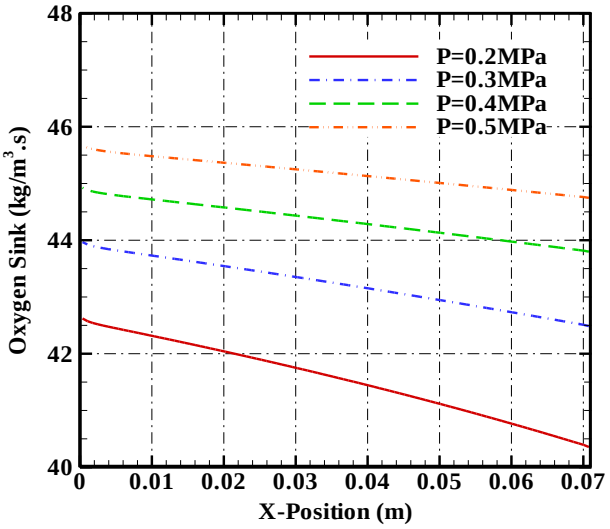

Fig. 5 The distribution of the oxygen sink at middle of catalyst layer for different fuel cell pressure

Fig. 6 shows the characteristic curves of PEM fuel cells which include fuel cell polarization and output power density. As it can be seen, the fuel cell characteristic curves shift positively with the increase of pressure.

As it was observed in Fig. 5, the increase of pressure increases the oxygen consumption rate in the cathode catalyst layer. Therefore according to the Faraday law, the local current generation rate increases. As a result, the PEM fuel cell output current density increases, which can obviously be seen in Fig. 6.

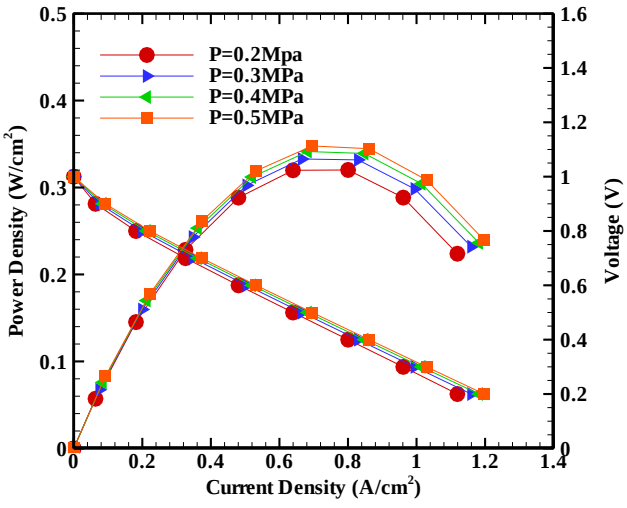

Fig. 6 Performance curves for different fuel cell pressure

Fig. 7 demonstrates the variations of fuel cell local current density with respect to the operating temperature. As it can be observed, the generated local current density increases with the increase of operating temperature. The increase of temperature causes the increase of exchanged current density, and consequently the improvement of mass transport properties in catalyst layer, which is the reaction site. Therefore the local current generation is boosted.

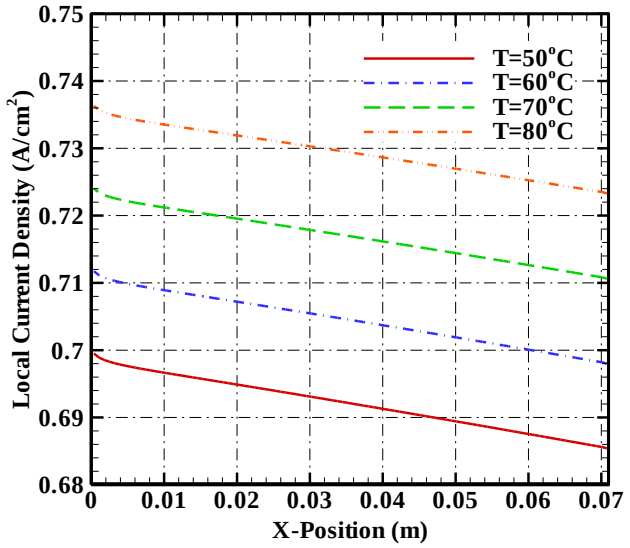

Fig. 7 The distribution of local current density at middle of catalyst layer for different fuel cell temperature

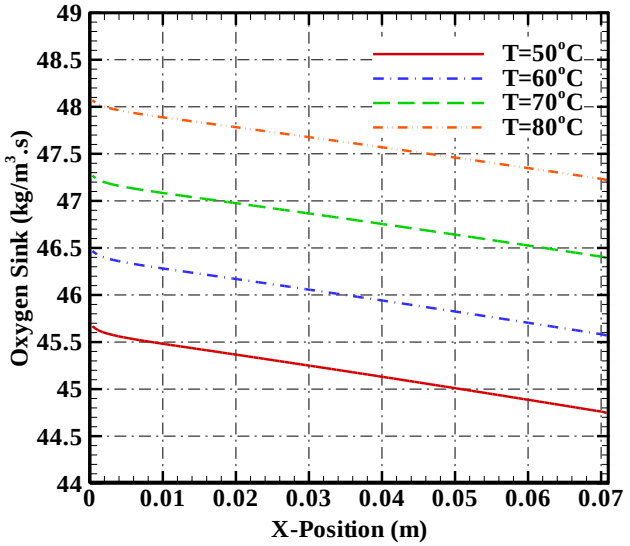

Fig. 8 The distribution of the oxygen sinks at middle of catalyst layer for different fuel cell temperatures

Fig. 8 shows the variations of oxygen sink term with respect to the PEM fuel cell operating temperature. Higher oxygen consumption rate can be seen in cathode side catalyst layer with the increase of fuel cell operating temperature, which shows the increase of local current generation rate. The variations of the PEM fuel cell characteristic curves with respect to the fuel cell operating temperature are shown in Fig. 9. As it was also observed in Fig. 8, the temperature increase causes the increase of oxygen consumption rate in cathode side catalyst layer, and therefore the PEM fuel cell output current density increases. Fig. 10 depicts the fuel cell local current density with respect to the cathode exchange coefficient. The increase of cathode exchange coefficient causes the reduction of the fuel cell voltage loss, and therefore the local current density in fuel cell increases.

Fig. 11 shows the variations of oxygen sink term with respect to the cathode exchange coefficient. As it can be seen, the increase of cathode exchange coefficient, for the sake of reaction rate boosting, increases the oxygen consumption rate. Fig. 12 shows the variations of fuel cell polarization and output power density with respect to the cathode exchange coefficient. As it was observed in Figs. 10 and 11, the increase of cathode exchange coefficient increases the oxygen consumption rate, and therefore, according to the Faraday law, the fuel cell local current generation increases. As a result, the PEM fuel cell output current density increases. The ohmic losses in fuel cell are due to the resistances in electrodes and various internal connections in the flow path of electrons and also due to the resistances in the transport path of positive ions in electrolyte. Fig. 13 shows the variations of local current density with respect to the fuel cell overall ohmic resistance. It is seen that with the increase of ohmic resistance, the fuel cell output current density reduces due to the higher resistances in the transport path of positive ions.

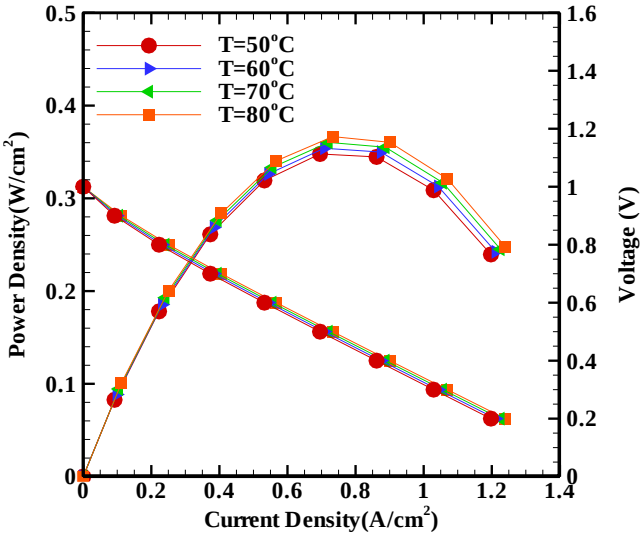

Fig. 9 Performance curves for different fuel cell temperature

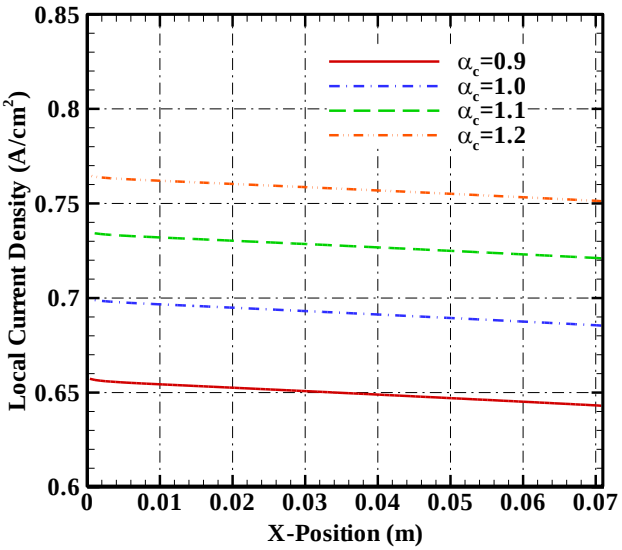

Fig. 10 The distribution of the local current density at middle of catalyst layer for different fuel cell cathode exchange coefficient

The variations of oxygen sink term with respect to the PEM fuel cell ohmic resistance is depicted in Fig. 14. The oxygen consumption rate in cathode catalyst layer increases with the increase of ohmic resistance.

Fig. 15 demonstrates the PEM fuel cell performance curves with respect to the overall ohmic resistance.

When the ohmic resistances increase, the resistance to the electron and proton transport in fuel cell increases. There-

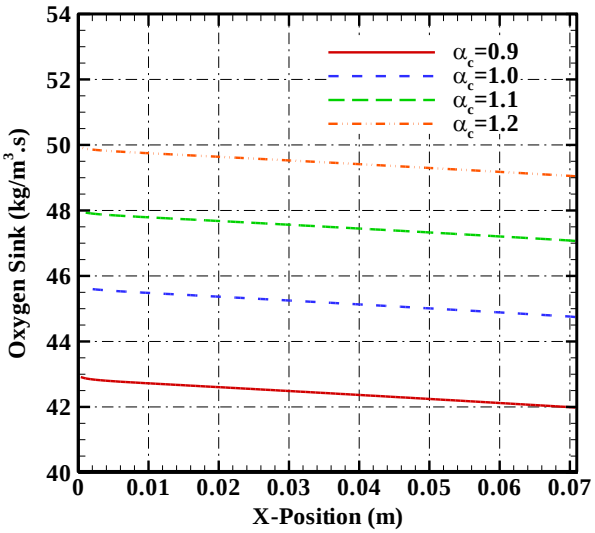

Fig. 11 The distribution of the oxygen sink at middle of catalyst layer for different fuel cell cathode exchange coefficient

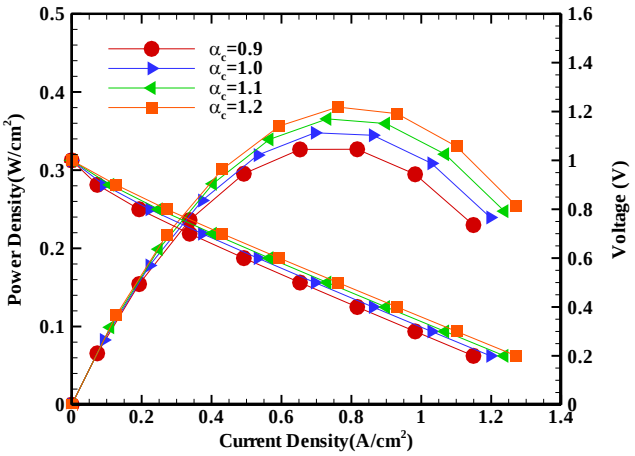

Fig. 12 The performance curves for different fuel cell cathode exchange coefficient

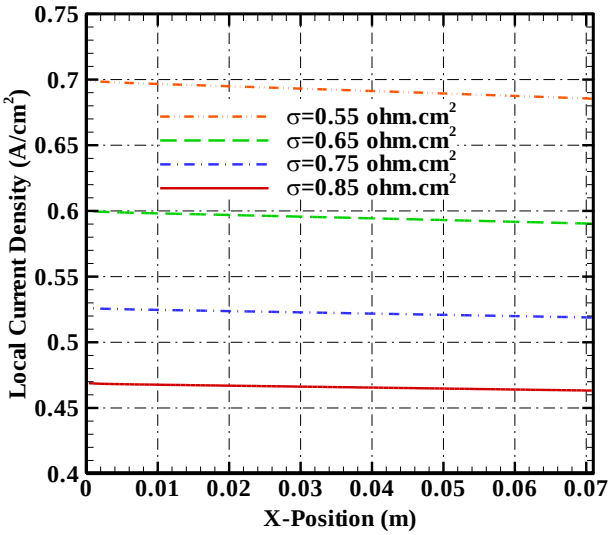

Fig. 13 The distribution of the local current density at middle of catalyst layer for different fuel cell overall ohmic resistance

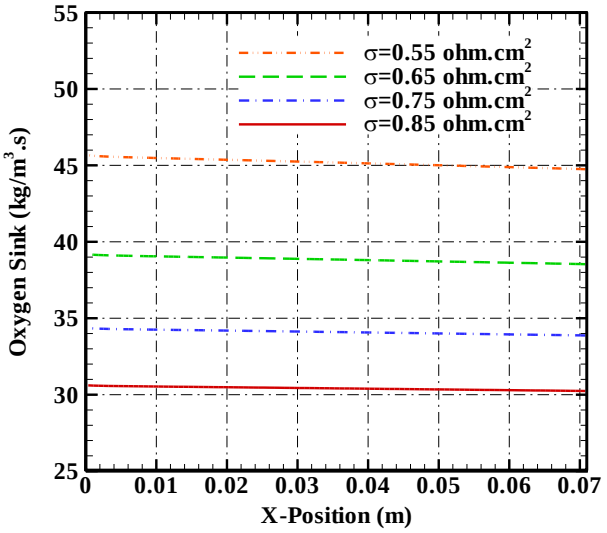

Fig. 14 The distribution of the oxygen sink at middle of catalyst layer for different fuel cell overall ohmic resistance

Table 2

The results for parametric study (V_{cell} = 0.5 V, $i \approx 0.696$ A cm^{-2})

Rank	Parameter	Ranges studied	Optimum value	Sensitivity Δi, A cm^{-2}	Sensitivity ΔP, W cm^{-2}
1	σ	0.55-0.85	0.55 Ω cm^2	0.227354386	0.113677193
2	α_C	0.9-1.2	1.2	0.108425761	0.054212881
3	P	2-5	5 atm	0.055977878	0.027988939
4	T	50-80	80°C	0.037486234	0.018743117
5	ε_{GDL}	0.2-0.5	0.5	0.019534051	0.009767026
6	U_{in}	0.1-0.7	0.7 m s^{-1}	0.019380243	0.009690121
7	H_{GDL}	0.0127-0.0508	0.0127 cm	0.01205766	0.00602883
8	$H_{channel}$	0.0381-0.1524	0.1524 cm	0.007391903	0.003695952
9	ε_{CL}	0.15-0.45	0.45	0.000695248	0.000347624
10	H_{CL}	0.000635-0.00254	0.000635 cm	0.000447686	0.000223843
11	K_{GDL}	1.76×10^{-10}-1.76×10^{-12}	1.76×10^{-10} m^2	5.9284E-05	2.9642E-05
12	K_{CL}	1.76×10^{-10}-1.76×10^{-12}	1.76×10^{-10} m^2	2.64E-07	1.32E-07

fore the fuel cell output power density decreases. The results of the parameter study are summarized in Table 2 in terms of the range, optimum value, and sensitivity for each parameter considered. The parameters are also ranked from 1 to 12 in order of their importance, with the rank 1 for σ indicating that it is the structural parameter that has the most significant influence on PEMFC performance.

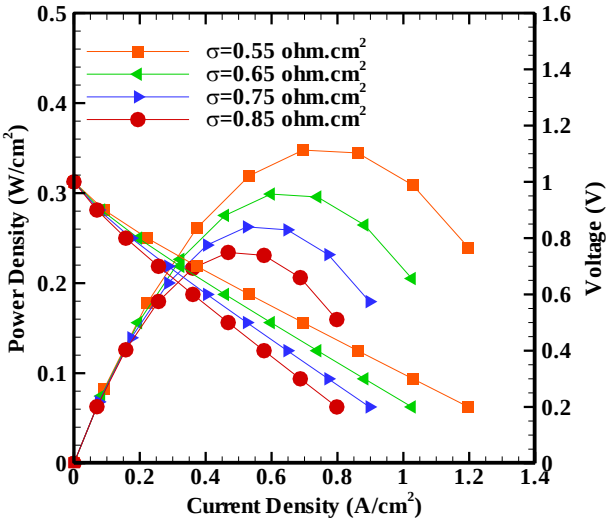

Fig. 15 Performance curves for different fuel cell overall ohmic resistance

7. Conclusions

A two-dimensional computational proton exchange membrane fuel cell (PEMFC) model is presented to investigate the effects of operating parameters such as overall ohmic resistance, cathode side charge transfer coefficient, operating pressure, and fuel cell temperature on PEMFCs. A single phase, compressible and isothermal flow of reactant-product mixture in the air-side electrode of PEMFC with straight gas channel is considered. The modeling results are illustrated using local current density curve, oxygen sink curve and performance curves. The results show that the net transport of reacting species through porous layers toward the catalyst layer and also the performance of PEMFC can be enhanced by increasing cathode side charge transfer coefficient, operating pressure and operating temperature. Also, σ (overall ohmic resistance) is the structural parameter that has the most significant influence on PEMFC performance.

Acknowledgement

Financial support from the Renewable Energy Organization of Iran (SUNA) is acknowledged.

References

1. **Wang, L.; Liu, H.** 2004. Performance studies of PEM fuel cells with interdigitated flow fields, J. Power Sources 134: 185-196. http://dx.doi.org/10.1016/j.jpowsour.2004.03.055.
2. **Jordan, L.R.; Shukla, A.K.; Behrsing, T.; Avery, N.R.; Muddle, B.C.; Forsyth, M.** 2000. Diffusion layer parameters influencing optimal fuel cell performance, J. Power Sources 86: 250-254. http://dx.doi.org/10.1016/S0378-7753(99)00489-9.
3. **Sridhar, P.; Perumal, R.; Rajalakshmi, N.; Raja, M.; Dhathathreyan, K.S.** 2001. Humidification studies on polymer electrolyte membrane fuel cell, J. Power Sources 101: 72-78. http://dx.doi.org/10.1016/S0378-7753(01)00625-5.
4. **Gurau, V.; Liu, H.; Kakac, S.** 1998. Two-dimensional model for proton exchange membrane fuel cells, AIChE J. 44: 2410-2422. http://dx.doi.org/10.1002/aic.690441109.
5. **Sun, W.; Pepply, B.A.; Karan, K.** 2005. An improved two-dimensional agglomerate cathode model to study the influence of catalyst layer structural parameters, Electrochim Acta 50: 3359-3374. http://dx.doi.org/10.1016/j.electacta.2004.12.009.
6. **Litster, S.; Pharoah, J.G.; McLean, G.; Djilali, N.** 2006. Computational analysis of heat and mass transfer in a micro-structured PEMFC cathode, J. Power Sources 156: 334-344. http://dx.doi.org/10.1016/j.jpowsour.2005.05.064.
7. **Khakbaz Baboli, M.; Kermani, M.J.** 2008. A two-dimensional, transient, compressible isothermal and two-phase model for the air-side electrode of PEM fuel cells, Electrochemica Acta 53: 7644-7654. http://dx.doi.org/10.1016/j.electacta.2008.04.017.
8. **Incropera, F.P.; DeWitt, D.P.; Bergman, T.L.; Lavine, A.S.** 2007. Fundamentals of Heat and Mass Transfer, John Wiley & Sons, 6th edition, 1024 p.
9. **Bernardi, D.M.; Verbrugge, M.W.** 1991. Mathematical model of a gas diffusion electrode bonded to a polymer electrolyte, AIChE J. 15: 13-24.
10. **Falcão, D.S.; Gomes, P.J.; Oliveira, V.B.; Pinho, C.; Pinto, A.M.F.R.** 2011, 1D and 3D numerical simulations in PEM fuel cells, Int. J. Hydrogen Energy 36: 12486-12498.
11. **Ticianelli, E.A.; Derouin, C.R.; Redondo, A.; Srinivasan, S.** 1988. Methods to advance technology of proton exchange membrane fuel cells, J. Electrochem. Soc. 135(9): 2209-2214. http://dx.doi.org/10.1149/1.2096240.
12. **You, L.; Liu, H.** 2006. A two-phase flow and transport model for PEM fuel cells, J. Power Sources 155: 219-230. http://dx.doi.org/10.1016/j.jpowsour.2005.04.025.
13. **Khajeh-Hosseini-Dalasm, N.; Fushinobu, K.; Okazaki, K.** 2010. Three-dimensional transient two-phase study of the cathode side of a PEM fuel cell, Int. J. Hydrogen Energy 35: 4234-4246. http://dx.doi.org/10.1016/j.ijhydene.2010.02.060.
14. **Khajeh-Hosseini-Dalasm, N.; Kermani, M.J.; Ghadiri Moghaddam, D;. Stockie, J.M.** 2010. A parametric study of cathode catalyst layer structural parameters on the performance of a PEM fuel cell, Int. J. Hydrogen Energy 35: 2417-2427. http://dx.doi.org/10.1016/j.ijhydene.2009.12.111.

M. Dehsara, M. J. Kermani

EKSPLOATACINIŲ PARAMETRŲ ĮTAKA PROTONŲ MAINŲ MEMBRANŲ KURO ELEMENTŲ FUNKCIONAVIMUI

R e z i u m ė

Pasiūlytas dvidimensis skaičiuojamasis protonų mainų membranos kuro elemento modelis (PAMKEM), siekiant ištirti tokius funkcionavimo rodiklius, kaip ominė varža, katodo pusės krūvininkų pernešimo koeficientas, darbinis slėgis ir kuro elemento temperatūros įtaka. Tiriamas reaktyvo ir produkto mišinio vienfazis, spūdusis ir izoterminis srautas tiesiame dujų kanale, kuro elemento protonų mainų membranos išorinėje pusėje. Mišinys susideda iš trijų dalių: deguonies, vandens garų ir azoto. Šiame straipsnyje aprašytas tipinis trisluoksnis modelis, kuris susideda iš katodo pusės dujų srauto kanalo ir katodo pusės katalizatoriaus sluoksnio. Skaičiavimams naudojamas dviejų paketų Gambit-Fluent programų junginys, siekiant išspręsti šį prognostinį modelį naudojant SIMPLE algoritmą, vaizduojantį modeliavimo rezultatus lokaline srovės tankio kreive, deguonies nugrimzdimo kreive ir atitikimo kreivėmis, apimančiomis *I–V* ir *I–P* kreives. Rezultatai rodo, kad reaktyviosios terpės tinklelio perdavimas per akytąjį sluoksnį į katalizės sluoksnį, taip pat PAMKEM efektyvumas gali būti padidinti didinant katodo pusės krūvininko perdavimo koeficientą, darbinį slėgį ir darbinę temperatūrą. Taip pat yra ištirta bendra ominė varža (σ), kuri yra struktūrinis parametras, turintis daugiausia įtakos PAMKEM funkcionavimui.

M. Dehsara, M.J. Kermani

THE EFFECTS OF OPERATING PARAMETERS ON THE PERFORMANCE OF PROTON EXCHANGE MEMBRANE FUEL CELLS

S u m m a r y

A two-dimensional computational proton exchange membrane fuel cells (PEMFCs) model is presented to investigate the effects of operating parameters such as overall ohmic resistance, cathode side charge transfer coefficient, operating pressure, and fuel cell temperature on PEMFCs. A single phase, compressible and isothermal flow of reactant-product mixture in the air-side electrode of PEM fuel cell with straight gas channel is considered. The mixture is composed of three species: oxygen, water vapor and nitrogen. The model presented in this paper is a typical three-layer that consists of cathode-side gas flow channel, cathode-side gas diffusion layer and cathode-side catalyst layer. For the present computation the assembly of the software packages Gambit+Fluent is used to solve this predictive model through SIMPLE algorithm and the modeling results are illustrated via local current density curve, oxygen sink curve and performance curves including *I–V* and *I–P* curves. The results reveal that the net transport of reacting species through porous layers toward the catalyst layer and also the performance of PEMFC can be enhanced by increasing cathode side charge transfer coefficient, operating pressure and operating temperature. Also the overall ohmic resistance (σ) is investigated which is the structural parameter that has the most significant influence on PEMFC performance.

Keywords: proton exchange membrane fuel cell, computational fluid dynamics, operating parameters.

Received September 19, 2012
Accepted November 11, 2013